



Ultrafine Ru nanoparticles embedded in SiO_2 nanospheres: Highly efficient catalysts for hydrolytic dehydrogenation of ammonia borane

Qilu Yao ^a, Weimei Shi ^b, Gang Feng ^c, Zhang-Hui Lu ^{a,d,*}, Xiaoliang Zhang ^a, Duanjian Tao ^a, Dejing Kong ^c, Xiangshu Chen ^{a,*}

^a Jiangxi Inorganic Membrane Materials Engineering Research Centre, College of Chemistry and Chemical Engineering, Jiangxi Normal University, Nanchang 330022, PR China

^b Sichuan Research Center of New Materials, Institute of Chemical Materials, China Academy of Engineering Physics, Mianyang 621900, PR China

^c Shanghai Research Institute of Petrochemical Technology SINOPEC, Shanghai 201208, PR China

^d CAS Key Laboratory for Biomedical Effects of Nanomaterials and Nanosafety, Institute of High Energy Physics, Chinese Academy of Sciences, Beijing 100049, PR China



HIGHLIGHTS

- Ru@SiO_2 core–shell NPs are synthesized via a simple one-pot synthetic route.
- Ultrafine Ru NPs (~ 2 nm) embedded in well-proportioned SiO_2 nanospheres (~ 25 nm).
- Ru@SiO_2 shows a high activity and good durability for H_2 generation from NH_3BH_3 .
- The measured activation energy 38.2 kJ mol^{-1} is lower than most of the reported values.

ARTICLE INFO

Article history:

Received 6 July 2013

Received in revised form

5 January 2014

Accepted 28 January 2014

Available online 12 February 2014

Keywords:

Core shell

Ammonia borane

Hydrogen generation

Hydrolysis

ABSTRACT

Ru@SiO_2 core–shell structured nanospheres have been prepared via a one-pot synthetic route in a NP-5/cyclohexane reverse micelle system and characterized by XRD, SEM, TEM, N_2 adsorption–desorption, and H_2 temperature programmed desorption. The characterized results show that ultrafine Ru nanoparticles (NPs) of around 2 nm are effectively embedded in the center of well-proportioned spherical and porous silica nanospheres (~ 25 nm in diameter). Interestingly, the number of Ru NPs increases inside the spherical particles of SiO_2 as the increase of Ru loading. The as-synthesized Ru@SiO_2 exhibits high catalytic activity and good durability for hydrogen generation from the aqueous of ammonia borane (AB) complex under ambient atmosphere at room temperature. The hydrolysis activation energy of Ru@SiO_2 was estimated to be about 38.2 kJ mol^{-1} , which is lower than most of the reported activation energy values for the same reaction using many different Ru-based and other noble metal containing catalysts, indicating the superior catalytic performance of these core–shell structured nanospheres.

© 2014 Elsevier B.V. All rights reserved.

1. Introduction

With increasing consumption of the fossil fuels, hydrogen energy has attracted more and more attention. The search for safe and efficient hydrogen storage materials remains one of the most difficult challenges on the way to a hydrogen-powered society as a long-term solution to solve energy problems [1–6]. Ammonia

borane (NH_3BH_3 , AB) is a stable white solid with a hydrogen storage capacity as high as 19.6 wt.%, exceeding that of gasoline and making itself an attractive candidate for chemical hydrogen storage [7–11]. The release of hydrogen from AB can be obtained through thermal dehydrogenation in solid state [12,13], and hydrolysis [7,10,14] or methanolysis [15–17] in solution. Generally speaking, thermal dehydrogenation process requires high temperature and power consumption. In contrast, ammonia borane is able to release hydrogen via a room temperature hydrolysis reaction in the presence of a suitable catalyst. Various transition metal catalysts, such as noble metals Rh [18,19], Ru [19–25], Pd [19,25–28], Pt [18,19,29], Au [19,30], non-noble metals Fe [31–33], Co [4,31,34–37], Ni [4,37–41], Cu [31,37,42–44] have been tested for hydrogen generation

* Corresponding authors. Jiangxi Inorganic Membrane Materials Engineering Research Centre, College of Chemistry and Chemical Engineering, Jiangxi Normal University, Nanchang 330022, PR China.

E-mail addresses: luzh@jxnu.edu.cn, zhanghuilu@gmail.com (Z.-H. Lu), cxs66cn@jxnu.edu.cn (X. Chen).

from the hydrolysis of NH_3NH_3 , among which Ru has been considered as one of the most active ones. However, most of these transition metal catalysts in nano-size are easily aggregated, resulting in a visible decrease in catalytic activity.

Recently, synthesis of metal NPs in a porous material or in a core–shell system has received much attention due to the possibility of obtaining monodisperse and ultrafine NPs [35,40,45–49]. The encapsulation of metal NPs in these systems can hinder the interaction between metal NPs and keep the active metal NPs stable even under harsh conditions. Nanoparticles (NPs) within silica spheres have attracted increasing interest in the fields of catalysis [50,51], absorbents [52,53], photonics [54,55] and magnetics [56,57]. Various approaches have been adopted to prepare such materials, however, besides the tedious assembly procedures, the sizes of metal NPs in silica spheres are often limited by the pre-synthesized metal colloids methods, as a result of the difficulty to prepare and assemble metal NPs smaller than 10 nm.

Herein, for the first time, we report a simple one-pot synthesis of Ru@ SiO_2 core–shell nanospheres, with ultrafine Ru NPs (around 2 nm) embedded in the center of the well-proportioned spherical particles of SiO_2 (around 25 nm). The present method completely avoids the metal NPs aggregate through the protection of silica. Especially, the as-prepared Ru@ SiO_2 catalysts exhibit high catalytic activity and good recycle stability for catalytic dehydrogenation from the aqueous of ammonia borane (AB) complex under ambient atmosphere at room temperature.

2. Experimental

2.1. Chemicals

All chemicals were commercially obtained and used without further purification. Ammonia borane (NH_3BH_3 , Aldrich, 90%), sodium borohydride (NaBH_4 , Sigma–Aldrich, 99%), ruthenium(III) chloride hydrate ($\text{RuCl}_3 \cdot x\text{H}_2\text{O}$, Aladdin Industrial Inc, 38–42 wt.% Ru basis), tetraethoxysilane (TEOS, Sigma–Aldrich, 98%), polyethylene glycolmono-4-nonylphenyl ether $n \approx 5$ (NP-5, TCI), ammonia solution ($\text{NH}_3 \cdot \text{H}_2\text{O}$, Nanchang Chemical Works, 28%), cyclohexane (C_6H_{12} , Tianjin Fuchen Chemical Reagent, >99.5%), methanol (CH_3OH , Tianjin Fuchen Chemical Reagent, 99.5%), and acetone ($(\text{CH}_3)_2\text{CO}$, Nanchang Chemical Works, >99.5%) were used as received. Ultrapure water with the specific resistance of 18.3 $\text{M}\Omega \text{ cm}$ was obtained by reversed osmosis followed by ion exchange and filtration.

2.2. Catalyst preparation

2.2.1. Synthesis of ruthenium NPs embedded in silica (Ru@ SiO_2)

The Ru@ SiO_2 nanospheres were prepared via a one-pot synthetic route (Fig. S1) by reversed-micelle technique as follows: calculated amounts of aqueous solutions of $\text{RuCl}_3 \cdot x\text{H}_2\text{O}$ (2.16 mL, corresponding to 1.0, 2.0, 4.0, 6.0, 8.0, and 10.0 wt.% Ru loading) were rapidly injected into 480 mL of NP-5 (20.16 g) cyclohexane solution. After stirring at room temperature for about 15 h, an aqueous ammonia solution (28 wt.%, 2.16 mL) was injected rapidly and after 2 h, TEOS (2.49 mL) was added rapidly. The solution was stirred for 2 days at room temperature. The as-synthesized silica nanospheres were isolated by addition of methanol to destabilize the reversed-micelle system and centrifugation at 10,000 rpm for 8 min. The product obtained was further washed with cyclohexane and acetone. Then the as-synthesized Ru@ SiO_2 catalysts were reduced by freshly aqueous solution of NaBH_4 (260 mM, 10 mL). The solid Ru@ SiO_2 was obtained by drying in vacuum oven at 313 K overnight.

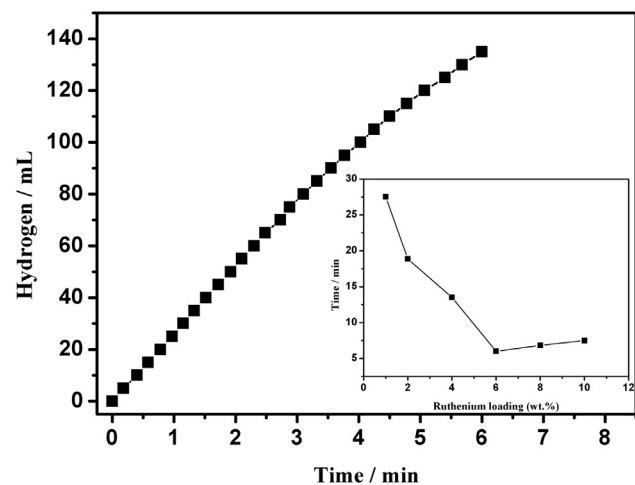


Fig. 1. Hydrogen generation from hydrolysis of NH_3BH_3 (200 mM, 10 mL) by the Ru@ SiO_2 nanospheres (Ru loading = 6 wt.% and $[\text{Ru}] = 0.5 \text{ mM}$) at 298 K. The inset shows the reaction time vs. the loading of ruthenium.

2.2.2. Synthesis of ruthenium NPs supported on silica (Ru/ SiO_2)

The Ru/ SiO_2 NPs in this study were prepared by the conventional impregnation method. The commercial SiO_2 (specific surface area = $200 \text{ m}^2 \text{ g}^{-1}$, Degussa, 99.8 %) were stirred in 10 mL of an aqueous solution of $\text{RuCl}_3 \cdot x\text{H}_2\text{O}$ (corresponding to 6 wt.% loading) for 12 h at room temperature. Then the as-synthesized Ru/ SiO_2 catalysts were reduced by freshly aqueous solution of NaBH_4 (260 mM, 10 mL). The solid Ru/ SiO_2 was obtained by drying in vacuum oven at 313 K overnight.

2.3. Catalyst characterization

Powder X-ray diffraction (XRD) studies were performed on a Rigaku RINT-2200 X-ray diffractometer with a $\text{CuK}\alpha$ source (40 kV, 20 mA). The morphologies and sizes of the samples were observed by using a transmission electron microscope (TEM, JEM-2010) equipped with an energy dispersive X-ray detector (EDX) for elemental analysis. The TEM samples were prepared by depositing one or two droplets of the nanoparticle suspensions on to the amorphous carbon coated copper grids. Scanning electron microscope (SEM) images were carried out on a SU8020 cold field-emission instrument. Surface area measurements were taken by N_2 adsorption at liquid nitrogen temperature using automatic volumetric adsorption equipment (Belsorp mini II). Hydrogen temperature programmed desorption ($\text{H}_2\text{-TPD}$) experiments were performed on a Micromeritics AutoChem II 2920 system, and the active surface area (S_{Ru}) was obtained by hydrogen chemisorption on the same instrument.

2.4. Catalytic hydrolysis of ammonia borane

The catalytic activity of the as-synthesized Ru@ SiO_2 or Ru/ SiO_2 toward hydrolytic dehydrogenation of the ammonia borane was evaluated in a typical water-filled graduated burette system. Typically, ammonia borane (NH_3BH_3 , 68.6 mg, Aldrich, 90%), and catalysts were placed in a two-necked round-bottomed flask. One neck of the flask was connected to a gas burette to measure the volume of hydrogen. The reaction started when 10 mL distilled water was injected into the mixture using a syringe and the evolution of gas was monitored using the gas burette. The reaction was completed when there was no more gas generation. The reactions were carried out at different temperatures (293 K–318 K) with Ru@ SiO_2 under

ambient atmosphere. For the durability test of the catalysts, after the first run of hydrogen generation reaction was completed, another equivalent of NH_3BH_3 (68.6 mg, 90%) was subsequently added to the reaction system and the released gas was monitored by the gas burette. The reactions were repeated 5 times under ambient atmosphere at room temperature. After hydrolysis reaction test, the catalysts were separated from the reaction solution by centrifugation, washed with water for three times and dried in vacuum oven at 313 K overnight.

3. Results and discussion

3.1. Catalytic dehydrogenation of ammonia borane

Fig. 1 shows the hydrogen generation from an aqueous NH_3BH_3 (200 mM, 10 mL) solution in the presence of Ru@SiO_2 (Ru loading = 6 wt.% and $[\text{Ru}] = 0.5 \text{ mM}$) at room temperature. The catalyst exhibits excellent activity to hydrolysis of NH_3BH_3 , generating its theoretic amount of hydrogen (135 mL) in only 6 min. The present catalytic hydrolysis reaction can be briefly expressed as follows: $\text{NH}_3\text{BH}_3 + 2\text{H}_2\text{O} \rightarrow \text{NH}_4^+ + \text{BO}_2^- + 3\text{H}_2$ [18]. The theoretical yield of hydrogen via this hydrolysis reaction is about 135 mL. Fig. 1 (inset) shows the hydrogen evolution from hydrolysis of an aqueous NH_3BH_3 (200 mM, 10 mL) solution in the presence of the Ru@SiO_2 nanospheres with various ruthenium loadings (1.0, 2.0, 3.0, 4.0, 6.0, 8.0, and 10.0 wt.%). The concentration of ruthenium is kept as a constant of 0.5 mM in all of the experiments under the same reaction conditions. Obviously, the catalysts demonstrate different catalytic activities with various ruthenium loadings. The reaction time first decreases with the increase of the ruthenium loadings and reaches the minimum at 6 wt.%, and then the reaction time slightly increases with the continuing increase of the ruthenium loadings. However, the molar ratio of hydrolytic generated hydrogen to the initial NH_3BH_3 is 3.0 in the presence of each catalyst, implying that all the catalysts with various Ru loadings have high catalytic activity for hydrolysis of AB to release theoretic amount of hydrogen. Ru@SiO_2 with a Ru loading of 6 wt.% displays the best catalytic performance for the generation of hydrogen amongst all the catalysts. The total turnover frequency (TOF) values of Ru@SiO_2 nanospheres with Ru loading of 1, 2, 4, 6, 8, and 10 wt.% are measured to be 44, 64, 89, 200, 176, and 160 $\text{mol H}_2 \text{ min}^{-1} \text{ mol}^{-1} \text{ Ru}$, respectively, for the hydrogen generation from the hydrolysis of AB (Table S1). The TOF value of Ru@SiO_2 (Ru: 6 wt.%) is lower than that of Ru/CB and Ru@MWCNT (Table S2) [20,22], but still higher than that of most reported noble metal catalysts for the same reaction at room temperature (Table S2) [19,20,22–26,58–60,62].

Fig. 2 shows the plots of the volume of hydrogen generated versus time during the catalytic hydrolysis of AB (200 mM, 10 mL) solution in the presence of Ru@SiO_2 catalysts (Ru loading = 6 wt.%) with different ruthenium concentrations (0.125, 0.25, 0.5, and 1.0 mM) at room temperature. When the ruthenium concentration increased, the reaction time catalyzed by Ru@SiO_2 nanospheres decreased obviously from 25.15 min to 3.52 min for complete hydrogen release. The hydrogen generation rate was determined from the linear portion of the plot for each ruthenium concentration. The plot of hydrogen generation rate vs. ruthenium concentration in logarithmic scale is shown in the inset of Fig. 2. The slope of the line is 0.92, which is closed to 1, indicating that the catalyzed hydrolytic dehydrogenation of ammonia borane by the Ru@SiO_2 nanospheres is first-order with respect to the catalyst concentration. The total turnover frequency (TOF) values of Ru@SiO_2 nanospheres with different Ru concentrations of 0.125, 0.25, 0.5, and 1.0 mM are measured to be 190, 196, 200, and 170 $\text{mol H}_2 \text{ min}^{-1} \text{ mol}^{-1} \text{ Ru}$, respectively, for the hydrogen generation from the hydrolysis of AB (Table S3).

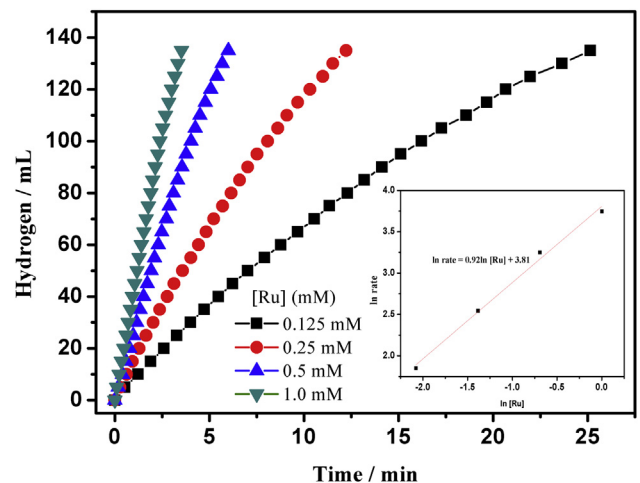


Fig. 2. Hydrogen generation from hydrolysis of NH_3BH_3 (200 mM, 10 mL) by the Ru@SiO_2 nanospheres (Ru loading = 6 wt.%) for the different concentration of Ru at 298 K. The inset shows the plot of hydrogen generation rate vs. the concentration of Ru, both in logarithmic scale.

Fig. 3 exhibits the time course of the hydrogen generation from AB (200 mM, 10 mL) in the presence of the Ru NPs embedded in silica (Ru@SiO_2) and Ru NPs supported on silica (Ru/SiO_2). The catalytic results demonstrated that the reaction rate significantly depended on the catalysts. As shown in Fig. 3, a stoichiometric amount of hydrogen (135 mL) was evolved in 6 min and 23 min, respectively, in the presence of the Ru@SiO_2 and Ru/SiO_2 NPs. Clearly, the Ru@SiO_2 core–shell nanospheres exhibited superior performance, in comparison to Ru/SiO_2 NPs, for the dehydrogenation of AB at room temperature. The high activity of the Ru@SiO_2 could be attributed to the encapsulation of Ru NPs in SiO_2 , which can hinder the interaction between metal NPs and keep the active metal NPs stable. While Ru NPs supported on the surface of SiO_2 are easily aggregated, resulting in loss of Ru surface area (Figs. S2, S3).

To explore the activation energy (E_a) of the NH_3BH_3 hydrolysis catalyzed by Ru@SiO_2 nanospheres, a series of experiments with different reaction temperatures were performed at constant molar ratio of Ru/AB. Fig. 4 shows the volume of hydrogen generated versus reaction time in the hydrolysis of NH_3BH_3 (200 mM, 10 mL) catalyzed by Ru@SiO_2 nanospheres (Ru loading = 6 wt.% and

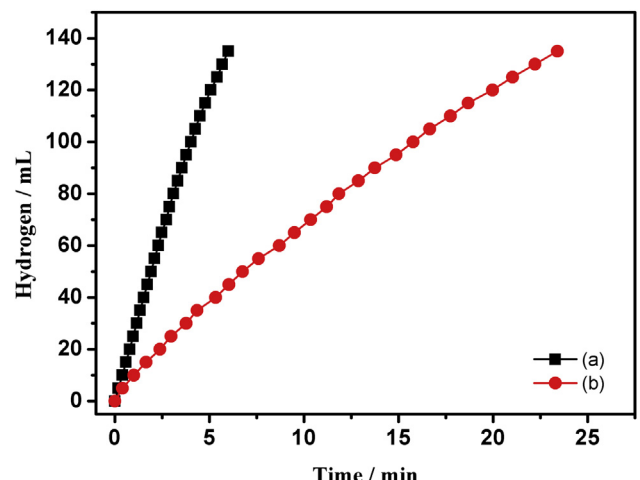


Fig. 3. Hydrogen generation from hydrolysis of NH_3BH_3 (200 mM, 10 mL) by (a) Ru@SiO_2 , (b) Ru/SiO_2 at 298 K (Ru = 0.5 mM).

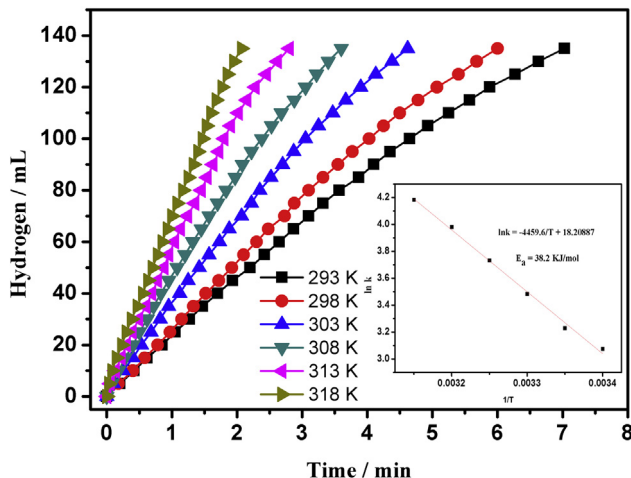


Fig. 4. Hydrogen generation from hydrolysis of NH_3BH_3 (200 mM, 10 mL) by the Ru@SiO_2 nanospheres (Ru loading = 6 wt.% and $[\text{Ru}] = 0.5$ mM) at 293–318 K. The inset shows the Arrhenius plot ($\ln k$ vs. $1/T$).

$[\text{Ru}] = 0.5$ mM) catalysts at various temperatures in the range of 293–318 K. As the temperature increases, the hydrogen generation rate rises gradually. The reaction rate constant k at different temperatures was estimated from the slope of the linear part of each plot in Fig. 4. The Arrhenius plot of $\ln k$ versus $1/T$ for the catalyst is plotted in Fig. 3 (inset). From the slope of the straight line, the activation energy (E_a) for the dehydrogenation of AB is estimated to be 38.2 kJ mol⁻¹, which is lower than most of the reported E_a values of many different Ru-based and other noble metal containing catalysts (Table 1) [19,20,22–26,29,58–66], exhibiting the superior catalytic performance of Ru@SiO_2 core–shell structured nanospheres.

The stability or durability is very important for the practical application of catalysts. In this sense, the reusability tests of the Ru@SiO_2 nanospheres (Ru loading = 6 wt.% and $[\text{Ru}] = 0.5$ mM) were performed. Fig. 5 shows the volume of hydrogen versus reaction time for the generation of hydrogen from an aqueous ammonia borane (200 mM, 10 mL) solution under ambient atmosphere at room temperature. Even after 5 runs of hydrolysis, the

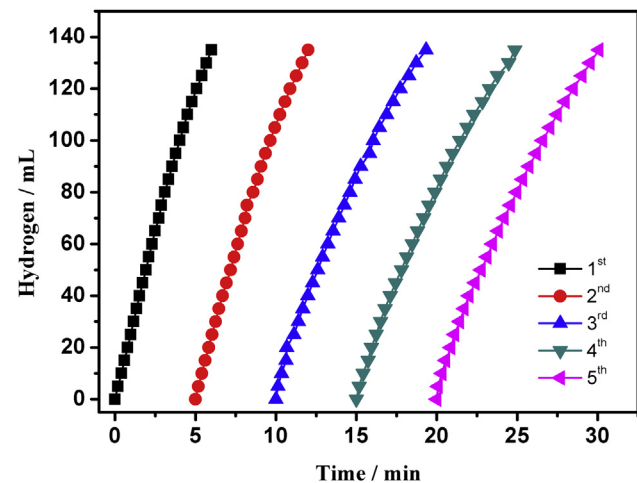


Fig. 5. The volume of hydrogen vs. reaction time for the generation of hydrogen from NH_3BH_3 solution (200 mM, 10 mL) catalyzed by the Ru@SiO_2 catalysts ($[\text{Ru}] = 0.5$ mM) at sequential runs by the addition of equivalent amounts of NH_3BH_3 .

activity of the catalysts has no obvious decrease, indicating that the Ru@SiO_2 core–shell structured nanospheres show good recycle stability for hydrogen generation from the aqueous of ammonia borane (AB) complex. In addition, a scale-up experiment reveals that the activity of the Ru@SiO_2 nanospheres has remained almost unchanged (Fig. S4), further indicating that the Ru@SiO_2 nanospheres has high catalytic activity.

3.2. Catalyst characterization

Powder X-ray diffraction (XRD) was performed on all the Ru@SiO_2 core–shell structured nanospheres after hydrolysis of ammonia borane. As shown in Fig. 6, all the XRD profiles for the sample of Ru@SiO_2 nanospheres show only the strong and the broad peaks in the range of $2\theta = 15\text{--}35^\circ$, which is assigned to be amorphous SiO_2 . Yet, the XRD profiles show no diffraction line to any ruthenium species (Fig. 6), probably due to the ruthenium particles size being too small.

Fig. 7 shows the SEM images of Ru@SiO_2 nanospheres after hydrolysis of NH_3BH_3 . The broad view of the sample given by the SEM images shows the uniform size and well-proportioned spherical particles of Ru@SiO_2 nanospheres. To better understand the morphologies and sizes, Ru@SiO_2 nanospheres with different Ru loadings were characterized by using a transmission electron

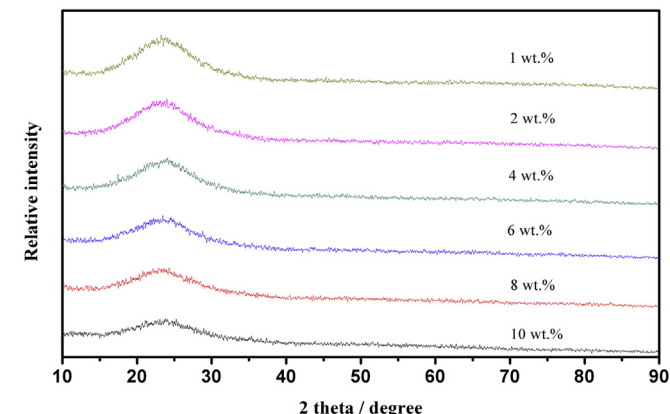


Fig. 6. Powder X-ray diffraction patterns for the Ru@SiO_2 nanospheres.

Table 1

The values of activation energy (E_a) for the hydrolysis of AB catalyzed by different catalysts.

Catalyst	E_a (kJ mol ⁻¹)	Ref.
Ru/carbon	76	[24]
Zeolite stabilized Rh	67	[58]
Ru/hydroxyapatite	59	[60]
Zeolite confined Pd	56	[61]
Pd–PVP– TiO_2	55	[29]
Pd/hydroxyapatite	54.8 ± 2	[62]
PSSA-co-MA stabilized Ru	54	[25]
RuCo/ γ - Al_2O_3	52	[63]
AgNi alloys	51.5	[65]
Pd/reduced graphene oxide (RGO)	51 ± 1	[26]
Ru/carbon black (CB)	49	[66]
Ru@ Al_2O_3	48	[59]
RuCu/ γ - Al_2O_3	47	[63]
Laurate-stabilized Ru	47	[23]
Ni@Ru/CB	44	[66]
Hollow Ru NPs/CB	39 ± 3	[64]
Ru@ SiO_2	38.2	This work
Ru/CB	34.81	[22]
Ru@MWCNT	33 ± 2	[20]
Ru/ γ - Al_2O_3	23	[19]

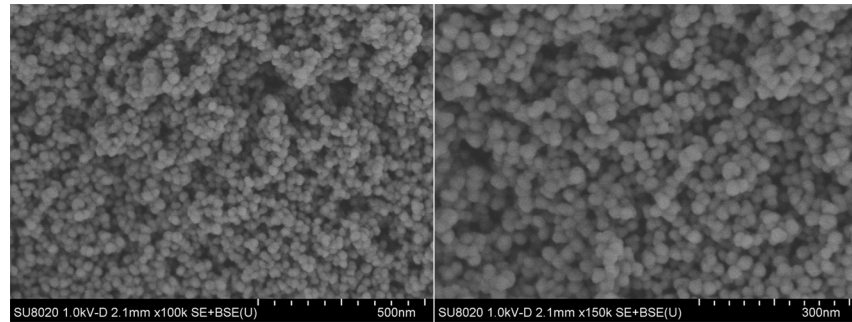


Fig. 7. SEM images of the Ru@SiO₂ nanospheres.

microscope (TEM) combined with an energy dispersive X-ray detector (EDX). TEM images for Ru/SiO₂ shown in Fig. S2 reveal the presence of partially aggregated NPs of irregular shape with the particle size of around 10 nm. As shown in Fig. 8a–d, the TEM images for Ru@SiO₂ clearly reveal that Ru NPs of around 2 nm are effectively embedded in the center of well-proportioned spherical particles of SiO₂ (~25 nm in diameter), in good agreement with SEM observation (Fig. 7). Interestingly, when the Ru loading increases, the number of Ru NPs increases inside the spherical particles of SiO₂ (Fig. 8a–d). However, when the ruthenium loading further increases to 10 wt.%, a small part of Ru NPs on the surface of silica nanospheres were observed. Fig. S5 exhibits the EDX spectra of the region marked in Fig. 8a. The EDX spectra shows K α peaks corresponding to O (0.53 keV), Si (1.74 keV), Ru (2.58, 19.26 keV) elements, and Cu signals (0.93, 8.04, 8.95 keV) from the TEM grids.

The EDX analysis confirms that monodisperse and ultrafine ruthenium nanoparticles inside the SiO₂ nanospheres.

The hydrogen temperature programmed desorption (H₂-TPD) curves for Ru@SiO₂ and Ru/SiO₂ shown in Fig. S3 imply that the Ru surface areas (S_{Ru}) are 15.4 and 8.7 m² g⁻¹, respectively, in line with the previous TEM characterization (Fig. 8 and Fig. S2) and catalytic activity test for the hydrolysis of AB (Fig. 3). Therefore, the calculated TOF values from Fig. 3 are 0.1285 and 0.0591 mol H₂ min⁻¹ m⁻² Ru, respectively, for Ru@SiO₂ and Ru/SiO₂ samples (Ru loading = 6 wt.%). Fig. 9 shows the nitrogen adsorption–desorption isotherms of the Ru@SiO₂ nanospheres after hydrolysis of ammonia borane. Ru@SiO₂ core–shell structured nanospheres have a high Brunauer–Emmett–Teller (BET) surface area of 193 m² g⁻¹. The type II isotherms with a small hysteresis loop occur at a relative pressure of 0.8–1.0 (Fig. 9), showing the

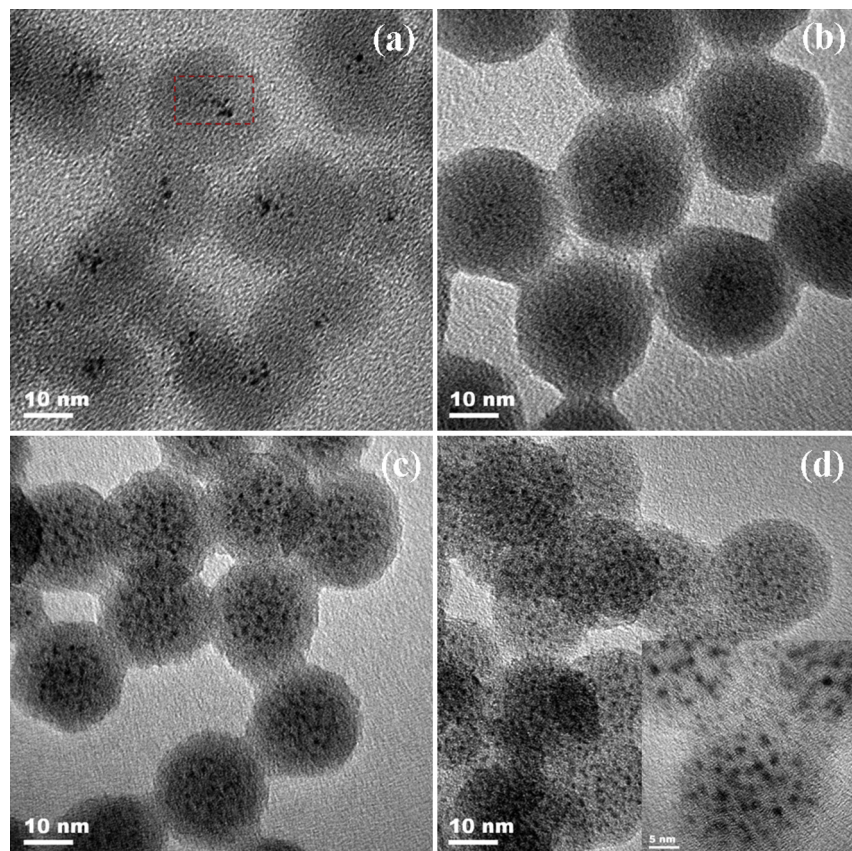


Fig. 8. Representative TEM images of the Ru@SiO₂ nanospheres with different ruthenium loadings (a) 1 wt.%, (b) 2 wt.%, (c) 6 wt.%, (d) 10 wt.%.

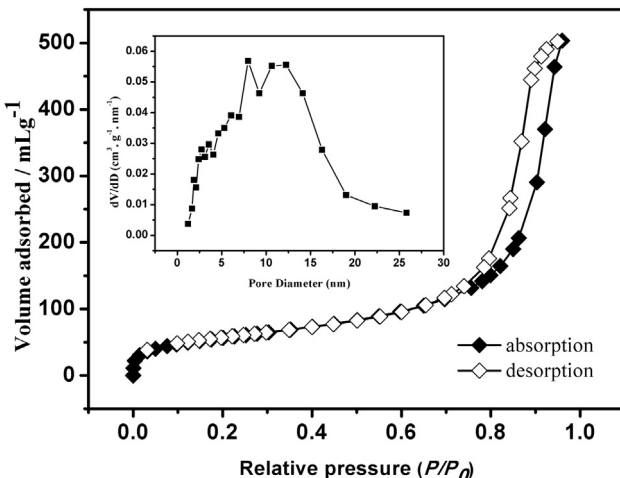


Fig. 9. Nitrogen adsorption–desorption isotherms of the Ru@SiO₂ nanospheres. The inset shows the pore size distribution of the Ru@SiO₂ nanospheres.

existence of mesopores and/or macropores in the samples. As shown in the inset of Fig. 9, the corresponding pore size distribution reveals the irregular pores with a large pore diameter formed in the SiO₂ shells. The pore volume of the sample is 0.7668 cm g⁻¹. The results of characterization and catalytic hydrolysis of AB indicate that the silica shell can keep metal core NPs stable while allow the reactants and products in and out of the nanospheres.

4. Conclusions

In summary, Ru@SiO₂ core–shell structured nanospheres were successfully prepared via a simple one-pot synthesis by using RuCl₃·xH₂O as precursor in a NP-5/cyclohexane reverse micelle system at room temperature. Ruthenium nanoparticles of around 2 nm were effectively embedded in the center of silica, and the number of Ru NPs increases inside the spherical particles of SiO₂ with the increase of Ru loading, confirmed by TEM and EDX characterization. Especially, Ru@SiO₂ exhibits high catalytic activity and excellent recycle stability for hydrogen generation from the aqueous of ammonia borane (AB) complex under ambient atmosphere at room temperature. The activation energy for the hydrolysis of NH₃BH₃ in the presence of Ru@SiO₂ was measured to be about 38.2 kJ mol⁻¹ from the evaluation of kinetic data at various temperatures, which is lower than most of the reported activation energy values of various Ru-based and other noble metal containing catalysts.

Acknowledgment

This work was financially supported by National Natural Science Foundation of China (No. 21103074), Natural Science Foundation of Jiangxi Province of China (No. 20114BAB203010 and 20132BAB203014), Jiangxi Provincial Department of Science and Technology (No. 2011BDH80023) and Jiangxi Provincial Education Department (No. GJJ12190). Z.-H. Lu was also supported by the “Gan-po talent 555” Project of Jiangxi Province and the Sponsored Program for Cultivating Youths of Outstanding Ability in Jiangxi Normal University.

Appendix A. Supplementary data

Supplementary data related to this article can be found at <http://dx.doi.org/10.1016/j.jpowsour.2014.01.122>.

References

- N.L. Rosi, J. Eckert, M. Eddaoudi, D.T. Vodak, J. Kim, M. O’Keeffe, O.M. Yaghi, *Science* 300 (2003) 1127–1129.
- X. Gu, Z.H. Lu, Q. Xu, *Chem. Commun.* 46 (2010) 7400–7402.
- U.B. Demirci, P. Miele, *Energy Environ. Sci.* 4 (2011) 3334–3341.
- Ö. Metin, S. Özkar, *Int. J. Hydrogen Energy* 36 (2011) 1424–1432.
- P. Chen, Z.T. Xiong, J.Z. Luo, J.Y. Lin, K.L. Tan, *Nature* 420 (2002) 302–304.
- G.A. Deluga, J.R. Salge, L.D. Schmidt, X.E. Verykios, *Science* 303 (2004) 993–997.
- C.W. Hamilton, R.T. Baker, A. Staibitz, I. Manners, *Chem. Soc. Rev.* 38 (2009) 279–293.
- Z.H. Lu, Q. Xu, *Funct. Mater. Lett.* 5 (2012) 1230001.
- M. Yadav, Q. Xu, *Energy Environ. Sci.* 5 (2012) 9698–9725.
- H.L. Jiang, Q. Xu, *Catal. Today* 170 (2011) 56–63.
- U.B. Demirci, P. Miele, *Energy Environ. Sci.* 2 (2009) 627–637.
- W. Grochala, P.P. Edwards, *Chem. Rev.* 104 (2004) 1283–1316.
- M. Ramzan, F. Silveira, A. Blomqvist, R.H. Scheicher, S. Lebegue, R. Ahuja, *Phys. Rev. B* 79 (2009) 132102.
- N. Mohajeri, A.T. Raissi, O. Adebiyi, *J. Power Sources* 167 (2007) 482–485.
- P.V. Ramachandran, P.D. Gagare, *Inorg. Chem.* 46 (2007) 7810–7817.
- H. Erdogan, Ö. Metin, S. Özkar, *Phys. Chem. Chem. Phys.* 11 (2009) 10519–10525.
- D.H. Sun, V. Mazumder, Ö. Metin, S.H. Sun, *ACS Catal.* 2 (2012) 1290–1295.
- M. Chandra, Q. Xu, *J. Power Sources* 156 (2006) 190–194.
- M. Chandra, Q. Xu, *J. Power Sources* 168 (2007) 135–142.
- S. Akbayrak, S. Özkar, *ACS Appl. Mater. Interfaces* 4 (2012) 6302–6310.
- G.P. Rachiero, U.B. Demirci, P. Miele, *Catal. Today* 170 (2011) 85–92.
- H. Liang, G. Chen, S. Desinan, R. Rosei, F. Rosei, D. Ma, *Int. J. Hydrogen Energy* 37 (2012) 17921–17927.
- F. Durap, M. Zahmakiran, S. Özkar, *Int. J. Hydrogen Energy* 34 (2009) 7223–7230.
- S. Basu, A. Brockman, P. Gagare, Y. Zheng, P.V. Ramachandran, W.N. Delgass, J.P. Gore, *J. Power Sources* 188 (2009) 238–243.
- Ö. Metin, S. Şahin, S. Özkar, *Int. J. Hydrogen Energy* 34 (2009) 6304–6313.
- P.X. Xi, F.J. Chen, G.Q. Xie, C. Ma, H.Y. Liu, C.W. Shao, J. Wang, Z.H. Xu, X.M. Xu, Z.Z. Zeng, *Nanoscale* 4 (2012) 5597–5601.
- Ö. Metin, E. Kayhan, S. Özkar, J.J. Schneider, *Int. J. Hydrogen Energy* 37 (2012) 8161–8169.
- Ö. Metin, S. Duman, M. Dinç, S. Özkar, *J. Phys. Chem. C* 115 (2011) 10736–10743.
- M. Rakap, E.E. Kalu, S. Özkar, *Int. J. Hydrogen Energy* 36 (2011) 1448–1455.
- J.M. Yan, X.B. Zhang, T. Akita, M. Haruta, Q. Xu, *J. Am. Chem. Soc.* 132 (2010) 5326–5327.
- Q. Xu, M. Chandra, *J. Power Sources* 163 (2006) 364–370.
- J.M. Yan, X.B. Zhang, S. Han, H. Shioyama, Q. Xu, *Angew. Chem. Int. Ed. Engl.* 47 (2008) 2287–2289.
- Z.H. Lu, J.P. Li, A.L. Zhu, Q.L. Yao, W. Huang, R.Y. Zhou, R.F. Zhou, X.S. Chen, *Int. J. Hydrogen Energy* 38 (2013) 5330–5337.
- U.B. Demirci, P. Miele, *J. Power Sources* 195 (2010) 4030–4035.
- T. Umegaki, J.M. Yan, X.B. Zhang, H. Shioyama, N. Kuriyama, Q. Xu, *J. Power Sources* 195 (2010) 8209–8214.
- J.M. Yan, X.B. Zhang, H. Shioyama, Q. Xu, *J. Power Sources* 195 (2010) 1091–1094.
- S.B. Kalidindi, M. Idirani, B.R. Jagirdar, *Inorg. Chem.* 47 (2008) 7424–7429.
- J.M. Yan, X.B. Zhang, S. Han, H. Shioyama, Q. Xu, *Inorg. Chem.* 48 (2009) 7389–7393.
- Ö. Metin, V. Mazumder, S. Özkar, S.H. Sun, *J. Am. Chem. Soc.* 132 (2010) 1468–1469.
- T. Umegaki, J.M. Yan, X.B. Zhang, H. Shioyama, N. Kuriyama, Q. Xu, *J. Power Sources* 191 (2009) 209–216.
- P.Z. Li, A. Ajaz, Q. Xu, *Angew. Chem. Int. Ed. Engl.* 51 (2012) 6753–6756.
- S.B. Kalidindi, U. Sanyal, B.R. Jagirdar, *Phys. Chem. Chem. Phys.* 10 (2008) 5870–5874.
- M. Zahmakiran, F. Durap, S. Özkar, *Int. J. Hydrogen Energy* 35 (2010) 187–197.
- M. Kaya, M. Zahmakiran, S. Özkar, M. Volkan, *ACS Appl. Mater. Interfaces* 4 (2012) 3866–3873.
- X. Gu, Z.H. Lu, H.L. Jiang, T. Akita, Q. Xu, *J. Am. Chem. Soc.* 133 (2011) 11822–11825.
- A. Ajaz, A. Karkamkar, Y.J. Choi, N. Tsumori, E. Ronnebro, T. Autrey, H. Shioyama, Q. Xu, *J. Am. Chem. Soc.* 134 (2012) 13926–13929.
- P.Z. Li, K. Aranishi, Q. Xu, *Chem. Commun.* 48 (2012) 3173–3175.
- H.L. Jiang, T. Umegaki, T. Akita, X.B. Zhang, M. Haruta, Q. Xu, *Chem. Eur. J.* 16 (2010) 3132–3137.
- Z.H. Lu, H.L. Jiang, M. Yadav, K. Aranishi, Q. Xu, *J. Mater. Chem.* 22 (2012) 5065–5071.
- S. Takenaka, H. Umebayashi, E. Tanabe, H. Matsune, M. Kishida, *J. Catal.* 245 (2007) 392–400.
- A.J. Zarur, J.Y. Ying, *Nature* 403 (2000) 65–67.
- T. Miyao, K. Minoshima, S. Naito, *J. Mater. Chem.* 15 (2005) 2268–2270.
- T. Miyao, K. Minoshima, Y. Kurokawa, K. Shinohara, W. Shen, S. Naito, *Catal. Today* 132 (2008) 132–137.
- P. Mulvaney, M. Giersig, T. Ung, L.M. Liz-Marzán, *Adv. Mater.* 9 (1997) 570–575.

[55] P. Yang, Z. Yuan, J. Yang, A. Zhang, Y. Cao, Q. Jiang, R. Shi, F. Liu, X. Cheng, *CrystEngComm* 13 (2011) 1814–1820.

[56] T. Haeiwa, K. Segawa, K. Konishi, *J. Magn. Magn. Mater.* 310 (2007) E809–E811.

[57] W.J. Li, X.X. Sha, W.J. Dong, Z.C. Wang, *Chem. Commun.* (2002) 2434–2435.

[58] M. Zahmakiran, S. Özkar, *Appl. Catal. B Environ.* 89 (2009) 104–110.

[59] H. Can, Ö. Metin, *Appl. Catal. B Environ.* 125 (2012) 304–310.

[60] S. Akbayrak, P. Erdek, S. Özkar, *Appl. Catal. B Environ.* 142–143 (2013) 187–195.

[61] M. Rakap, S. Özkar, *Int. J. Hydrogen Energy* 35 (2010) 1305–1312.

[62] M. Rakap, S. Özkar, *Int. J. Hydrogen Energy* 36 (2011) 7019–7027.

[63] G.P. Rachiero, U.B. Demirci, P. Miele, *Int. J. Hydrogen Energy* 36 (2011) 7051–7065.

[64] G. Chen, S. Desinan, R. Rosei, F. Rosei, D. Ma, *Chem. Commun.* 48 (2012) 8009–8011.

[65] C. Yao, L. Zhuang, Y. Cao, X. Ai, H. Yang, *Int. J. Hydrogen Energy* 33 (2008) 2462–2467.

[66] G. Chen, S. Desinan, R. Rosei, F. Rosei, D. Ma, *Chem. Eur. J.* 18 (2012) 7925–7930.